H2Open Journal

IWA PUBLISHING

222

H2Open Journal Vol 3 No 1
doi: 10.2166/h2oj.2020.117

Development of algorithms for evaluating performance of flood simulation models with satellite-derived flood

Tushar Surwase[a,*], P. Manjusree[a], Sachin Prakash[b] and Saikiran Kuntla[c]

[a] Special User Flood and Landslide Monitoring Division (SFLMD)/NRSC/ISRO, Hyderabad, 500037, India

[b] Application Software and Computing Infrastructure Division (ASCID)/NRSC/ISRO, Hyderabad, 500037, India

[c] Department of Civil Engineering, Indian Institute of Technology, Delhi (IIT-D), Delhi, 110016, India

*Corresponding author. E-mail: tusharsurwase@ymail.com

Abstract

Flood inundation simulation models are widely used for simulating severe events of flood, generating hazard maps, risk assessment, and to identify flood vulnerable locations. It is important to assess the degree of accuracy of flood model results as these results may be one of the triggering parameters considered in developing flood hazard maps, flood mitigation policies, and land using planning where multi-criteria analysis is approached. In the present study, an algorithm is developed in order to know the performance of flood models by validating it with flood footprints extracted from synthetic aperture radar (SAR) images using multi-segmentation and Otsu's thresholding technique. Evaluation of the performance of the model is based on two best fit criteria called F1 and F2. For this, HEC-RAS model is used for simulating the severe event of flood witnessed in Mahanadi River in Odisha stretching between Tikarpara and Mundali during September 2008. Three simulations were made by considering three different Manning's roughness for river and floodplain. The model gives appreciable results and best fit F1 = 0.85 and F2 = 0.74 was found for Manning's roughness 0.020.

Key words: evaluation, HEC-RAS, model performance, multi-segmentation and Otsu's thresholding

Highlights

- The study showcases development of algorithms for extraction of flood disaster footprints without any manual intervention which can help disaster respondents to respond to the event in near real time.
- It also showcases development of algorithms for evaluation performance of flood models which help flood modellers to evaluate the used flood model performance in validation with satellite-based observed flood.

INTRODUCTION

Flooding is a global phenomenon that causes human and property loss as mentioned by Teng *et al.* (2017). A flood inundation hydraulic model predicts flood extent and it may be an important source of information for flood risk assessment studies and in determining flood-vulnerable areas (Liu *et al.* 2018; Shastry & Durand 2019). Flood models also play an important role in flood preparedness and flood risk reduction as stated strongly by Chen *et al.* (2019). Flood hydrodynamic

H2Open Journal Vol 3 No 1
doi: 10.2166/h2oj.2020.117

models give the result in the form of depth, water surface elevation and velocities with respect to time. Researchers and hydraulic modelers simulate flood for a river basin to study its impact assessment and to design hydraulic structures. They generally validate their simulated flood extent results (total area) with observed flood extent (ground truth or satellite observed) total area. Validating by considering only total area simulated versus total area observed cannot be a correct practice because simulated extent may be more than observed extent at some places and at some places the reverse may be true. Thus, results compared in terms of total area may give appreciable results, however, there will be ambiguity in the validation. Hence, simply evaluating total area flood simulated versus total area flood observed cannot give a correct picture of hydraulic/flood model performance. The simulated results must be assessed pixel-wise with satellite observed extent in order to evaluate flood model performance. There are many statistical approaches for evaluating flood model performance, one of which was developed by SENAGUA (2014) to compare the water surface elevation result from the model to the ground scenario. Bates & De Roo (2000) evaluated the model performance based on flood extent. Horrit *et al.* (2007) and Di Baldassarre *et al.* (2009) worked on evaluating flood extent in terms of measures of fit F1 and F2 which was proposed for flood studies by Moya-Quirogaa *et al.* (2016). The present study uses Horrit and Di Baldassarre techniques, which were further modified to develop an algorithm in Python for evaluating the performance of flood model (F1 and F2) automatically by inputting two rasters, i.e., flood observed and flood simulated. This technique is selected as it evaluates flood extent in terms of measures of fit, which is limited to the scope of the present study. The significance of the developed algorithm over the existing technique is that the algorithm minimizes the number of GIS operations and computational efforts on two rasters (flood simulated and flood observed) in order to evaluate fitting values F1 and F2 and estimate cell values, which are correctly predicted, overpredicted, and underpredicted by the model. To test the algorithm, 2D flood simulation model is set up for part of Mahanadi River in Odisha in the HEC-RAS model. HEC-RAS (Hydrologic Engineering Centre – River Analysis System) is a freely available and popular hydraulic model developed by the United States Army Corps of Engineers (USACE). The flood inundation can be simulated by using 1D (one-dimensional) or 2D (two-dimensional) models. HEC-RAS version prior to 5.0.1 was limited to simulating 1D flow, which can be suitable to analyze the behavior of flow in open channels (natural or artificial) where water is flowing below danger level, and thus can be considered to be 1D flow as the water is flowing only in the longitudinal direction. When water levels exceed threat (danger) level and water approaches floodplains, there is the possibility of water moving in two directions, thus 2D flow modeling becomes essential for simulating floods with greater accuracy. Taking this into account, USACE in February 2016 developed version 5.0.1, which has the capability to simulate 2D flow. HEC-RAS is open source hydraulic software which performs better and achieves high accuracy in inundation modeling, Surwase *et al.* (2019) concluded in their flood inundation simulation study. The study uses HEC-RAS 2D model version 5.0.1 February 2016 release to simulate the floods for the September 2008 Mahanadi river flood. The simulations are performed by providing the daily river discharge values as an input which were recorded at the time of the flood event and obtained from Central Water Commission. The model shows the simulation results in the form of flood extent with depth and velocity. The results were further validated with RADARSAT SAR satellite image. SAR has proven to be an effective tool for water surface detection as stated by Tholey *et al.* (2015), Hoque *et al.* (2011), Henry *et al.* (2006), Kuenzer *et al.* (2013), for estimation of flood depth studied by Iervolino *et al.* (2015), and flooding beneath vegetation canopies in certain conditions observed by Richards *et al.* (1987), Hess *et al.* (1990), Townsend (2002a, 2002b), Kasischke & Bourgeau-Chavez (1997). Commonly used SAR-based flood extent mapping approaches include simple visual interpretation (Oberstadler *et al.* 1997), supervised classification (De Roo *et al.* 1999; Townsend 2002a, 2002b), image texture algorithms (Schumann *et al.* 2005), histogram thresholding (Schumann *et al.* 2010), various multitemporal change detection methods (Bazi *et al.* 2005), and active contour models (Bates *et al.* 1997; Matgen *et al.* 2007). Among these, Cao *et al.*

H2Open Journal Vol 3 No 1
doi: 10.2166/h2oj.2020.117

(2019) mentioned that histogram thresholding is a common and simple approach which can be used to separate flood and non-flood areas in a large area (swathe) due to the specular backscattering characteristics of active radar pulses on plain water surfaces and the resultant low signal return.

Visual inspection and manual editing can help in training regions of interest (ROIs) and reducing false positives/negatives, demonstrated by Pulvirenti *et al.* (2010). As manual editing is time-consuming and manpower-driven, it cannot be applied to rapid response to flood disasters, especially during back-to-back flood events (Shen *et al.* 2019). The common technique used is the thresholding technique which is a pixel-based operation and considered as the most efficient way for rapid mapping. The specular reflection properties of non-obstructed water have driven numerous endeavors to decide a limit, beneath which, pixels are recognized as water, which was demonstrated by Yamada (2001), Giustarini *et al.* (2013), Hirose *et al.* (2001), and Matgen *et al.* (2011). A single threshold may not hold well in large-area water bodies (Tan *et al.* 2004) or for the whole swathe of a SAR image since it suffers from the heterogeneity of the environment, caused by wind-roughening and satellite system parameters (Martinis *et al.* 2009). Martinis & Rieke (2015) demonstrated the temporal heterogeneity of the backscattering of permanent water bodies, implying the temporal variability of the threshold. To address the spatial variability, Martinis *et al.* (2009) applied a split-based approach (SBA) together with an object-oriented (OO) segmentation method as described by Baatz (1999). Matgen *et al.* (2011) introduced a histogram segmentation method, and Giustarini *et al.* (2013) generalized the calibration process. Pulvirenti *et al.* (2011) developed an image segmentation method consisting of dilution and erosion operators to remove isolated groups of water pixels and small holes in water bodies, which are believed to be caused by speckle. Giustarini *et al.* (2013), Matgen *et al.* (2011), and Lu *et al.* (2014) employed the region growing algorithm (RGA) to extend inundation areas from detected water pixels. The RGA starts from seeding pixels and then keeps absorbing homogenous pixels from neighbors until no more homogenous pixels exist in neighboring areas. Martinis *et al.* (2009) applied SBA, as described by Bovolo & Bruzzone (2007), to determine the global threshold for binary (water and non-water) classification. In SBA, a SAR image is first divided into splits (sub-tiles) to determine their individual thresholds using the Kittler and Illingworth (KI) method, global minimum, and quality index described by Kittler & Illingworth (1986). Then, only global threshold can be obtained by qualified splits showing sufficient water and non-water pixels.

In this study, automation of the delineation of the flood is carried out using a multi-segmentation technique combined with Otsu's threshold technique and executed with Python scripts. The post-processing component includes removal of stray pixels and applying a water mask to delineate the final flood layer. The GDAL module in Python was used to read the pre-processed image/intermediate product and water mask, along with their projection system. Later, the image is processed for classification with numpy and scikit-image modules. The final output is exported using GDAL module with the same input projection system.

STUDY AREA

The flood simulation was carried out for a stretch of the Mahanadi River in Odisha state, India. The study area is from Tikarpara to Mundali and lies between latitudes 20° 07′58.8″ N and 20° 43′8.4″ N and longitudes 84°44′42″ E and 85° 46′4.8″ E. Mahanadi is the major river flowing through Odisha state and in the study area. A location map of the study area is shown in Figure 1.

There are two gauge stations, Tikarapara and Mundali, where discharge is measured. The study area is located at the downstream side of Hirakud dam, which intercepts a catchment area of 48,700 km^2 that is responsible for floods in Mahanadi deltaic area (Parhi *et al.* 2012). Odisha witnessed peak floods in September 2008 affecting millions of people, damaging agricultural crops and infrastructure.

H2Open Journal Vol 3 No 1
doi: 10.2166/h2oj.2020.117

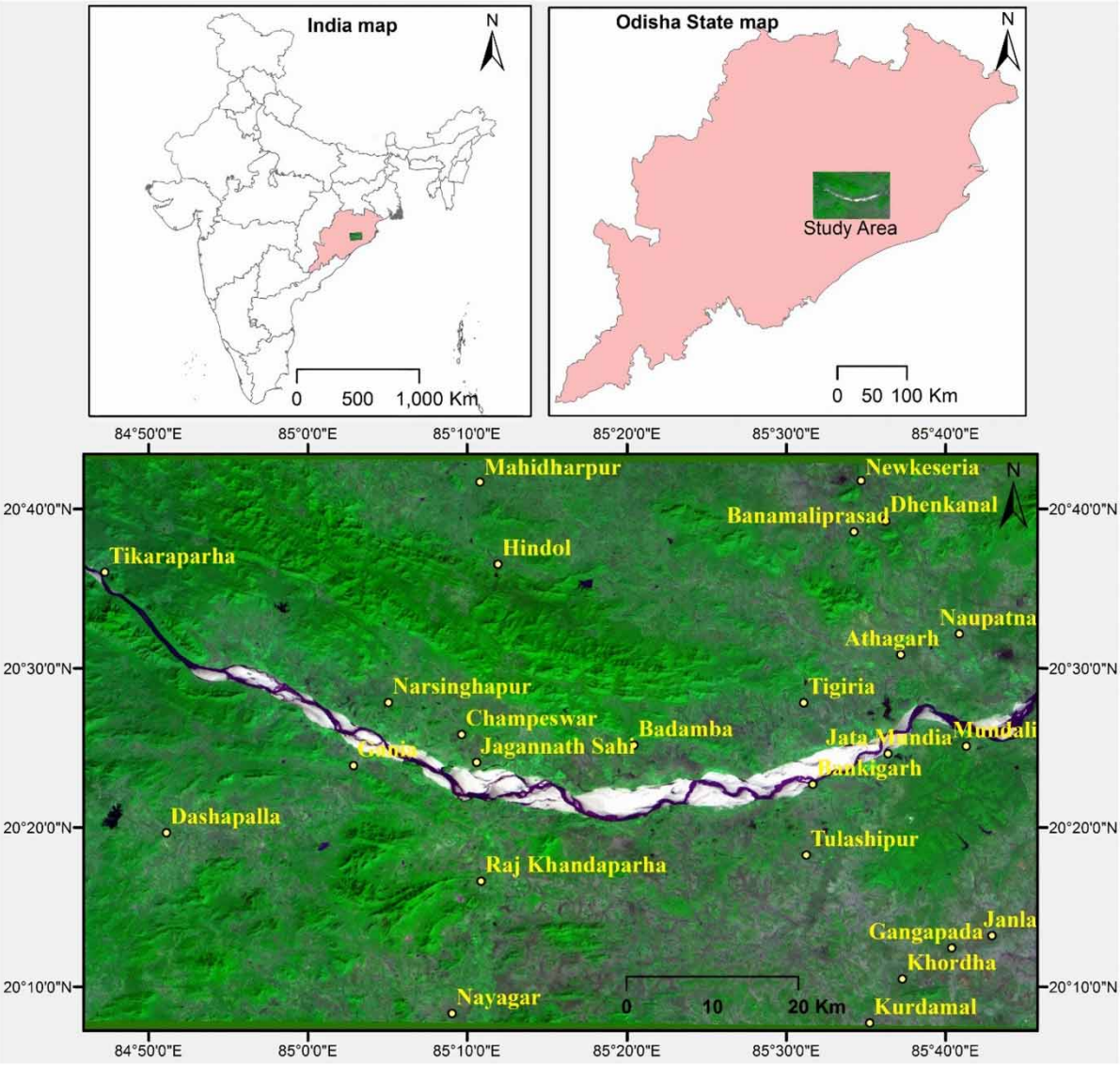

Figure 1 | Study area showing location map and major settlements (IRS-LISS-III image).

Hence, flood inundation simulation for the September 2008 flood event is carried out for the study area.

DATA USED

Flood inundation simulation was carried out by using Carto-DEM 10 meter spatial resolution. Land-use land cover (LULC) at 1:250,000 scale derived from Advanced Wide Field Sensor (AWiFS) image acquired in 2016–2017, was used for assigning Manning's roughness coefficient of the terrain. Discharge data collected from Central Water Commission (CWC) of Tikarpara gauge station were used as inflow boundary condition of the setup model in HEC-RAS. The study simulated the flood event between 2 September 2008 and 30 September 2008. Radarsat satellite SAR image was used to validate the simulated results.

H2Open Journal Vol 3 No 1
doi: 10.2166/h2oj.2020.117

METHODS

The methodology is split into three categories, namely, flood simulation, development of an algorithm for extraction of flood footprints from SAR image, and development of an algorithm for evaluating the performance of flood models.

2D flood simulation

Flood is simulated by using HEC-RAS version 5.0.1 for the flood event between 5 September and 30 September, 2008. The study area is defined by 2D closed polygon. The 2D polygon is an area where flood inundation is expected to occur. The polygon is digitized by connecting higher elevation like hills and mountains where flood inundation will not extend beyond the same features. After defining the boundary of a polygon, the computational square cells are generated. The cells are in a square grid called a staggered grid and at the boundary of the 2D polygon the cells are in a non-staggered grid which is a composition of polygons having three to a maximum of eight sides. The spacing of the square grid was kept at an interval 10 m × 10 m in x and y directions which was kept equal to spatial resolution of the digital elevation model (DEM) used. Further, two boundary conditions were assigned to the 2D polygon. The first one is the inflow boundary condition which represents observed discharge in the form of a hydrograph at Tikarpara gauge station. The observed inflow hydrograph in between the simulation period is shown in Figure 2. The width of the river at the gauge station is 760 m which covers 76 cells, and the inflow boundary condition was applied to these 76 cells. The second boundary condition is the outflow boundary condition normal depth assigned at Mundali station. Considering topographic conditions from DEM, normal depth slope 0.001 was assigned. Three simulations were carried out for three different roughness coefficients for river banks (floodplains), with roughness coefficient for the channel being kept the same for all three simulations (Table 1).

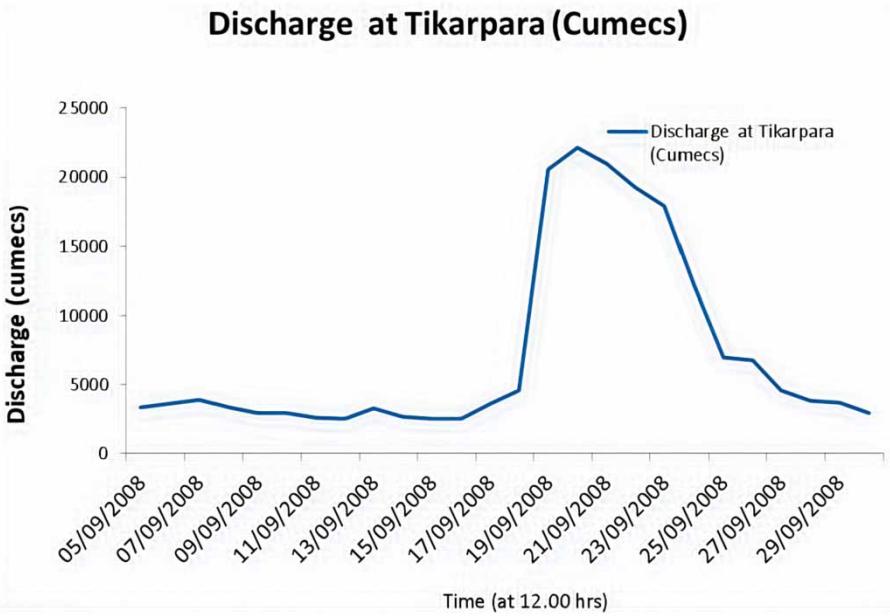

Figure 2 | Observed inflow hydrograph at Tikarpara gauge station.

H2Open Journal Vol 3 No 1
doi: 10.2166/h2oj.2020.117

Table 1 | Roughness coefficient for three simulations

Simulation	Roughness coefficient for channel (n_c)	Roughness coefficient for floodplains (n_p)
1	0.032	0.020
2	0.032	0.030
3	0.032	0.040

The simulation is carried out using full momentum Equations (1) and (2):

$$\frac{\partial p}{\partial t}+\frac{\partial}{\partial x}\frac{(p^2)}{(h)}+\frac{\partial}{\partial y}\frac{(pq)}{(h)}=-n^2pg\frac{\sqrt{(p^2+q^2}}{h^2}-gh\frac{\partial s}{\partial x}+pf+\frac{\partial}{\rho\partial x}(h\tau_{xx})+\frac{\partial}{\rho\partial y}(h\tau_{xy}) \tag{1}$$

$$\frac{\partial q}{\partial t}+\frac{\partial}{\partial x}\frac{(q^2)}{(h)}+\frac{\partial}{\partial y}\frac{(pq)}{(h)}=-n^2qg\frac{\sqrt{(p^2+q^2}}{h^2}-gh\frac{\partial s}{\partial y}+qf+\frac{\partial}{\rho\partial y}(h\tau_{yy})+\frac{\partial}{\rho\partial x}(h\tau_{xy}) \tag{2}$$

where, h is the water depth in meters, p and q are specific flow in x and y directions (m^2/sec), s is the surface elevation in meters, n is the Manning's resistance, g is gravitational acceleration in m/sec^2, ρ (rho) is the density of water in kg/m^3, f is the Coriolis force (/sec) and τ_{xx}, τ_{xy}, and τ_{yy} are the components of effective shear stress. Computational time step was evaluated based on the Courant–Friedrichs–Lewy condition given in Equation (3):

$$cr=\frac{C\,\Delta t}{\Delta x} \tag{3}$$

where, cr is Courant's number, c is celerity in m/sec; Δt is a computational time step in seconds, Δx is grid cell size in meters. The celerity 'c' was calculated considering the maximum depth of water observed at Tikarpara gauge station. Thus, Equation (3) can be returned as:

$$\frac{\sqrt{gh}}{\Delta x}\frac{\Delta t}{1}=\leq 1 \tag{4}$$

Since $c=\sqrt{gh}$, g is gravitational acceleration (m/sec^2) and h is the maximum depth of water observed at Tikarpara gauge station.

Development of algorithm for evaluating performance of flood simulation models

The developed algorithm is based on measure of fit of two raster datasets, i.e., simulated raster R1 and satellite-derived observed flood raster R2. Both of these rasters are of the order of one bit format. In order to find the correctly predicted cells (A), overpredicted cells (B), and underpredicted cells (C), the process starts with raster calculator $2 \times R1 - R2$. If the value of the cell is 1 then the corresponding cell values are correctly predicted. If the value of the cell is 2, then the corresponding cell values are overpredicted and if the value of the cell is -1, then the corresponding cell values are underpredicted. The evaluation is carried out using the formula shown by Equations (5) and (6). The performance evaluation algorithm was scripted/coded in ArcPy, which is available in the scripting module within Arc-Map (ArcGIS software module) version 10.6.1. The script requires a spatial analyst toolbox license and extension to execute the code. The map algebra function under the spatial analyst tool was used to extract the cells that are correctly predicted, underpredicted, and overpredicted. Code developed for performance evaluation of the flood model is shown in Figure 3. Figure 4 depicts the simulated layer, observed flood extent, correctly predicted, overpredicted, and underpredicted cells. The adopted methodology for evaluation of flood models is shown in Figure 5. The best fit

H2Open Journal Vol 3 No 1
doi: 10.2166/h2oj.2020.117

```
# Import arcpy module
import arcpy
from arcpy.sa import *
# Check out any necessary licenses
arcpy.CheckOutExtension("spatial")
#Modelled inundation raster
ras1 = "E:\Mahanadi_project_tushar\srtm30\p2\\depth.tif"
#Actual satellite inundation raster
ras2 = "E:\\Mahanadi_project_tushar\\fld1\\fld707aug.img"
#Temporary calculated raster
out_file = "E:\\Mahanadi_project_tushar\\fld1\\test1121"
#Check for pixel size compatibility for raster calculator
result = 2*Raster(ras1) - Raster(ras2)
result.save(out_file)
rows = arcpy.SearchCursor(out_file)
for row in rows:
    if row.getValue("VALUE") == -1: #Underestimated
        C = row.getValue("COUNT")
        print "count of underesti cells is %d" %C
    elif row.getValue("VALUE") == 2:  #Overestimated
        B = row.getValue("COUNT")
        print "count of overesti cells is %d" %B
    elif row.getValue("VALUE") == 1: #Correctly Predicted
        A = row.getValue("COUNT")
        print "count of correctly predi cells is %d" %A
rows_sat = arcpy.SearchCursor(ras2)
for row in rows_sat:
    if row.getValue("Value") == 1:
        tot_ras2 = row.getValue("Count")
        #print "count of total cells in satellite image
##C = tot_ras2 - A
##print "count of underesti cells is %d" %C
F1 = (float(A))/(float(A) + float(B) + float(C))
F2 = (float(A) - float(B))/(float(A) + float(B) + float(C))
print "The value of F1 is %f"  %F1
print "The value of F2 is %f"  %F2
```

Figure 3 | Code developed for performance evaluation of flood model.

value F1 and F2 is given by Equations (5) and (6), respectively.

$$F1 = A/(A + B + C) \tag{5}$$

$$F2 = (A - B)/(A + B + C) \tag{6}$$

The value of F1 ranges from 0 to 1; F2 value ranges from −1 to 1. If the value of F1 and F2 is closer to 1, it means that the model performance is better, and if F1 and F2 values are exactly 1, it means all the cells are correctly predicted and there is not a single cell which is under- or overpredicted.

Development of algorithm for extraction of flood footprints from SAR image

SAR images should be pre-processed before carrying out the analysis. The pre-processing steps include applying orbit file, calibration, speckle filtering, terrain correction, linear to decibel conversion, adding elevation band, and deriving land/water mask using GPT tool with the help of Python scripts. After pre-processing, the image is divided into segments, each of size 100×100 pixels. Each segment is further divided into four sub-segments of size 50×50 pixels. The size of segments and sub-segments was fixed after testing on more than 50 images of different areas. The procedure followed by Martinis *et al.* (2015) is used for the selection of segments automatically. The mean

H2Open Journal Vol 3 No 1
doi: 10.2166/h2oj.2020.117

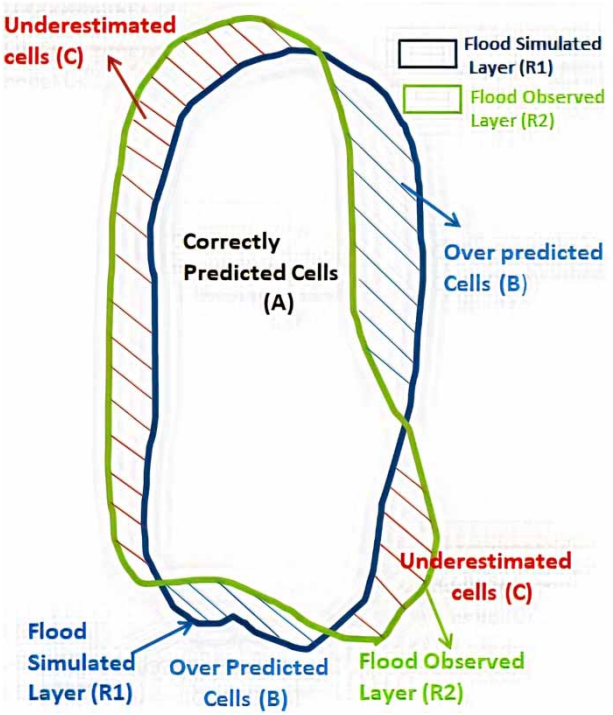

Figure 4 | Schematic diagram of flood simulated extent and observed flood extent.

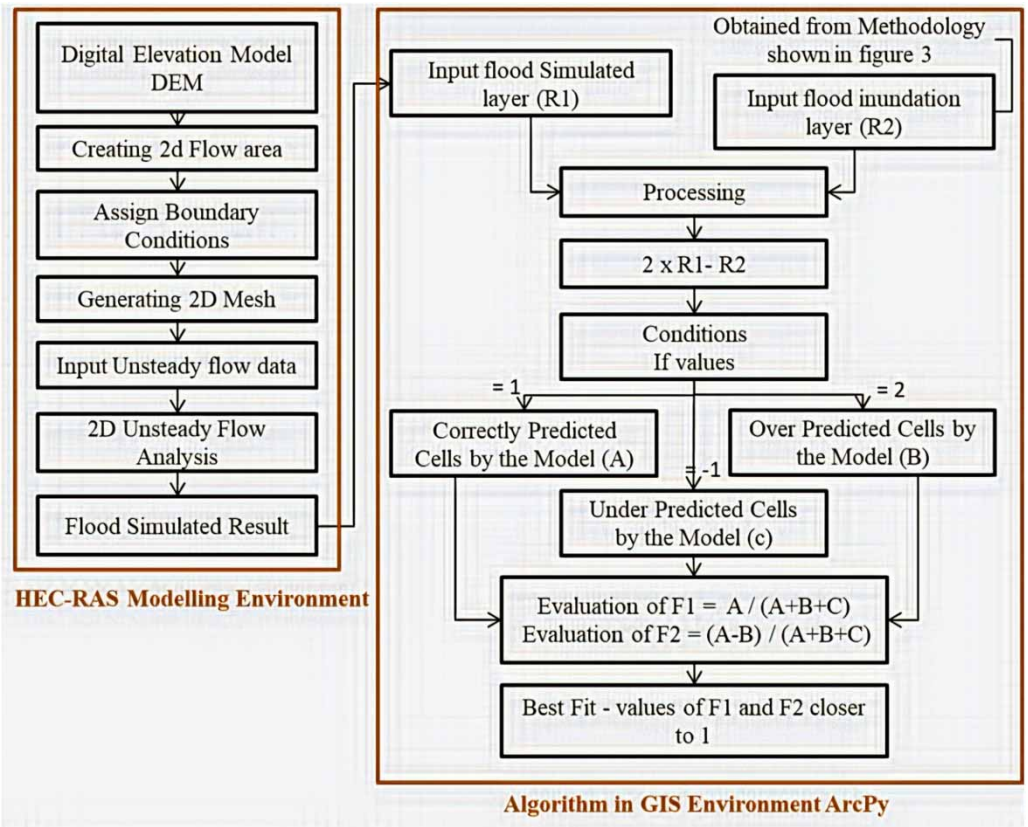

Figure 5 | Methodology flow chart for evaluation of flood models.

H2Open Journal Vol 3 No 1
doi: 10.2166/h2oj.2020.117

intensity values are calculated in each sub-segment and using the respective mean values of four sub-segments, the standard deviation of the segment is calculated. Two conditions were checked, namely, first, the standard deviation of the segment must be high (>95% quantile). This criterion helps in finding the segments where there is a greater probability of distribution of more than one class within it and the number of pixels of each class is of good ratio. Second, the mean intensity value of the segment must be less than the mean intensity value of the whole image. This ensures that the selected segments have a good number of water pixels. If the number of segments which are satisfying the above-mentioned conditions is less than five then the size of segments and sub-segments is reduced to half and the quantile for the choice of tile is reduced to (90%) make sure that the segments also are chosen having information of a comparatively low extent of water surfaces or with smaller spread water bodies. Further, the top five segments in terms of standard deviation are selected for further analysis, since that is sufficient for threshold computation (Twele *et al.* 2016).

Otsu's thresholding technique is used to automatically perform clustering-based image threshold (Sezgin & Sankur 2004). The algorithmic rule assumes that the SAR image contains two categories of pixels which follow a bi-modal bar-chart, termed as foreground and background pixels, it then evaluates the optimum threshold separating the two categories so that their combined spread (intra-class variance, defined as a weighted sum of variances of the two classes) is minimal, or equivalently, so that their inter-class variance is maximal by (Otsu 1979). This technique has been employed by Vala & Baxi (2013) as it is effective and found to give reliable results to discover the threshold for each segment which was selected in the previous stage. The arithmetic mean of the thresholds of the five selected segments is finally generated and it is used as the global threshold for applying to the whole image to get a preliminary classified image. The preliminary classified image is refined using SRTM 1Sec HGT DEM data, applying majority filter and water mask. The overclassified water pockets are eliminated using SRTM 1Sec HGT DEM data obtained in the pre-processing stage from the terrain-corrected input image and areas where elevation ought to be above 15 meters are eliminated and classified as water. This ultimately reduces the commission errors which are usually caused because of shadows in the hills. Majority filter is also known as mode/modal filter. It is used to replace the central pixel value within a pre-mentioned size kernel with the pixel value which is reiterated a number of times in the same kernel. This operation reduces the stray pixels on the preliminary classified image and produces a smoothened image. SRTM water mask of the study area is used to exclude the permanent water bodies so as to generate a flood layer. Figure 6 shows the methodology adopted

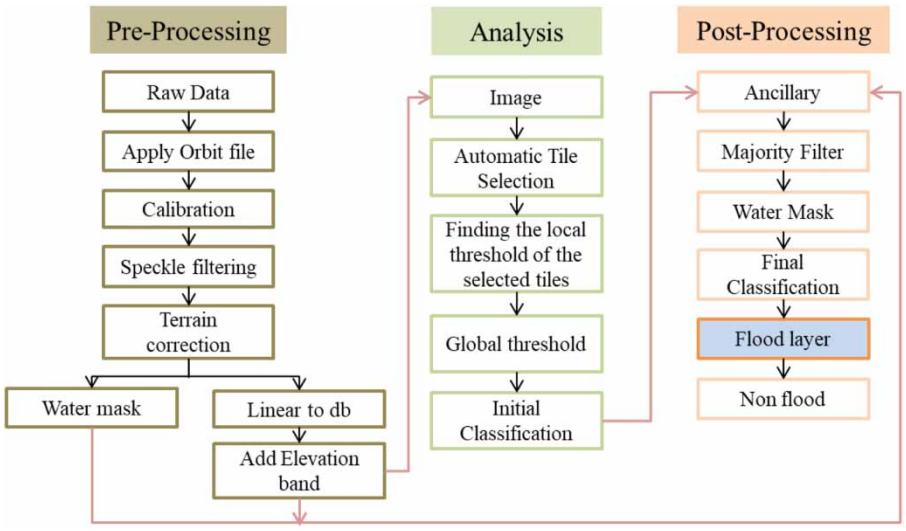

Figure 6 | Methodology flow chart for extraction of flood footprints from SAR image.

H2Open Journal Vol 3 No 1
doi: 10.2166/h2oj.2020.117

for extracting flood footprints from the SAR image. Table 2 shows the technical specifications of hardware and software used for automation.

Table 2 | Technical specifications of hardware and software used for automation

Programming language used	**Python**
Platform	Anaconda 3.7.1
System configuration	Intel i5 8th generation, 16 GB RAM
Modules used	GDAL, Numpy, Scikit-image, tkinter, matplotlib and Graph Processing Tool (GPT) by ESA's SNAP
Processing time	14 minutes

RESULTS AND DISCUSSION

HEC-RAS-simulated output results deliver temporal flood extent with depth, velocity of water, and surface water elevation. The simulated output results are stored in tiff file format with floating point type. The simulated output results can be generated for the desired date and time from the simulated period. For the present study, the simulated result for the desired date and time of 23 September, 2008 at 0600 hours was exported from the model to validate with RADARSAT satellite SAR data acquired on the same date and time. Delineated flood footprints from RADARSAT SAR image using multi-segmentation and Otsu's thresholding technique are shown in Figure 7. The flood simulated result for roughness coefficient 0.02 in floodplains is shown in Figure 8. Similarly, flood-simulated results for flood roughness coefficient 0.030 and 0.040 are shown in Figures 9 and 10,

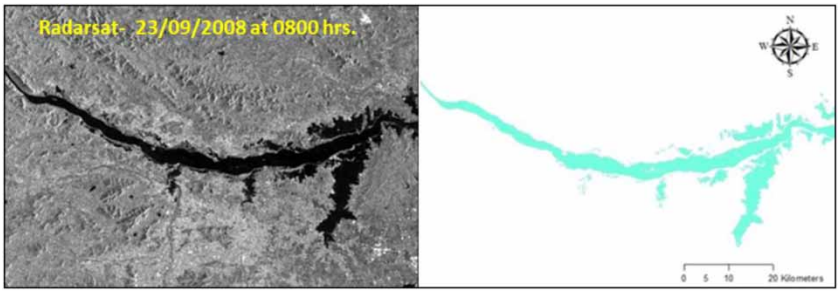

Figure 7 | RADARSAT SAR image (left) and its delineated flood layer (right).

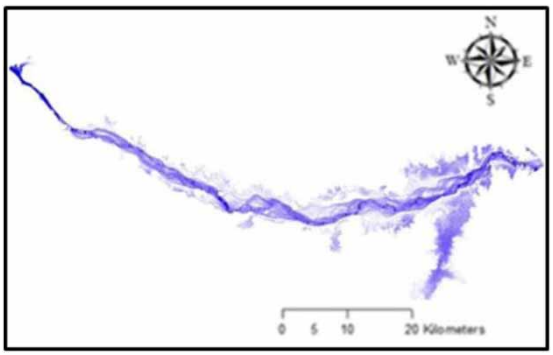

Figure 8 | Flood simulated by HEC-RAS on 23 September 2016 at 0,600 hours with Manning's roughness coefficient 0.020.

H2Open Journal Vol 3 No 1
doi: 10.2166/h2oj.2020.117

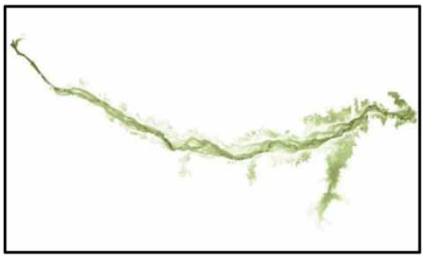

Figure 9 | Flood simulated results for roughness coefficient 0.030 for floodplains.

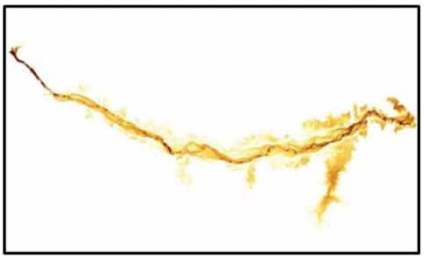

Figure 10 | Flood simulated results for roughness coefficient 0.040 for floodplains.

respectively. The F1 and F2 measures of fit have been evaluated for all three simulations using the algorithm and are shown in Tables 3 and 4. From the results, it is observed that F1 and F2 values are closer to 1 for the roughness coefficient 0.020 for floodplains when compared to others. Further, the inundated areas for simulated and observed is calculated by multiplying the number of pixels with a single pixel area (100 m^2) as 10 m is the spatial resolution. It is observed that the total inundated area for this coefficient is matching 94% with the simulated. as shown in Table 4.

Table 3 | Model performance for different roughness coefficients

Sr. no.	Manning's roughness coefficient n_c n_p		Correctly predicted flood cells 'A'	Over predicted flood cell 'B'	Under predicted flood cell 'C'	F1	F2
1	0.032	0.020	1,553,668	206,750	52,092	0.85	0.74
2	0.032	0.030	1,554,075	519,470	51,685	0.73	0.50
3	0.032	0.040	1,554,381	745,570	48,379	0.67	0.35

Table 4 | Flood inundated area observed vs. simulated

Sr. no.	Manning's Roughness coefficient n_c n_p		Flood observed (FO) hectares	Flood simulated (FS) hectares	F0/FS
1	0.032	0.020	17,057.6	18,125.10	0.94
2	0.032	0.030	17,057.6	21,252.30	0.80
3	0.032	0.040	17,057.6	23,483.30	0.72

CONCLUSION

The present study uses HEC-RAS model for simulating the severe flood event of Mahanadi River in Odisha. Three simulations were run using different Manning's coefficient for floodplains.

H2Open Journal Vol 3 No 1
doi: 10.2166/h2oj.2020.117

Satellite-based flood footprints were extracted by multi-segmentation and Otsu's thresholding technique which will be helpful for disaster responders to prepare flood hazard maps in near real time without any manual intervention. The development of an algorithm for performance evaluation of the HEC-RAS model for three different simulations in validation with extracted flood prints from RADARSAT shows appreciable results for Manning's roughness coefficient 0.020 for floodplains and 0.032 for channel as measures of fit F1 and F2 are 0.85 and 0.74, respectively, which are closest to 1 among the other two simulation values. From the results it is inferred that the HEC-RAS model is sensitive towards the Manning's roughness coefficient. The developed algorithm for performance evaluation can be used for any flood model (MIKE, Tuflow, ANUGA, etc.) which has the capability to export the flood inundation extent result in GIS formats.

DATA AVAILABILITY STATEMENT

All relevant data are included in the paper or its Supplementary Information.

REFERENCES

Baatz, M. 1999 Object-oriented and multi-scale image analysis in semantic networks. In: *Proceedings of the 2nd International Symposium on Operationalization of Remote Sensing*, 16–20 August 1999, Enschede, The Netherlands.

Bates, P. D. & De Roo, A. P. J. 2000 A simple raster-based model for flood inundation simulation. *J. Hydrol.* **236** (1–2), 54–77. https://doi.org/10.1016/S0022-1694(00)00278-X.

Bates, P. D., Horrit, M. S., Smith, C. N. & Mason, D. C. 1997 Integrating remote sensing observations of flood hydrology and hydraulic modelling. *Hydrological Processes* **11**, 1777–1795.

Bazi, Y., Bruzzone, L. & Melgani, F. 2005 An unsupervised approach based on the generalized Gaussian model to automatic change detection in multitemporal SAR images. *IEEE Trans. Geosci. Remote Sens.* **43**, 874–887.

Bovolo, F. & Bruzzone, L. 2007 A split-based approach to unsupervised change detection in large-size multitemporal images: application to tsunami-damage assessment. *IEEE Trans. Geosci. Remote Sens.* **45** (6), 1658–1670. doi:10.1109/tgrs.2007.895835.

Cao, H., Zhang, H., Wang, C. & Zhang, B. 2019 Operational flood detection using Sentinel-1 SAR data over large areas. *Water* **11**, 786. doi:10.3390/w11040786.

Chen, Z., Luo, J., Chen, N., Xu, R. & Shen, G. 2019 RFim: a real-time inundation extent model for large floodplains based on remote sensing big data and water level observations. *Remote Sens.* **11**, 1585.

De Roo, A., Van Der Knijff, J., Horritt, M., Schmuck, G. & De Jong, S. 1999 Assessing flood damages of the 1997 Oder flood and the 1995 Meuse flood. In: *Proceedings of the Second International ITC Symposium on Operationalization of Remote Sensing*, 16–20 August 1999, Enschede, The Netherlands.

Di Baldassarre, G., Schumann, G. & Bates, P. D. 2009 A technique for the calibration of hydraulic models using uncertain satellite observations of flood extent. *J. Hydrol.* **367**, 276–282. doi:10.1016/j.jhydrol.2009.01.020.

Giustarini, L., Hostache, R., Matgen, P., Schumann, G. J., Bates, P. D. & Mason, D. C. 2013 A change detection approach to flood mapping in urban areas using terrasar-x. *IEEE Trans. Geosci. Remote Sens.* **51**, 2417–2430.

Henry, J. B., Chastanet, P., Fellah, K. & Desnos, Y. L. 2006 Envisat multi-polarized ASAR data for flood mapping. *Int. J. Remote Sens.* **27**, 1921–1929.

Hess, L. L., Melack, J. M., Simonett, D. S. & Sieber, A. J. 1990 Radar detection of flooding beneath the forest canopy: a review. *Int. J. Remote Sens.* **11**, 1313–1325.

Hirose, K., Maruyama, Y., Do Van, Q., Tsukada, M. & Shiokawa, Y. 2001 Visualization of flood monitoring in the lower reaches of the Mekong River. In: *Proceedings of the 22nd Asian Conference on Remote Sensing*, 5–9 November 2001, Singapore.

Hoque, R., Nakayama, D., Matsuyama, H. & Matsumoto, J. 2011 Flood monitoring, mapping and assessing capabilities using RADARSAT remote sensing, GIS and ground data for Bangladesh. *Nat. Hazards* **57**, 525–548.

Horrit, M., Di Baldasarre, G., Bates, P. & Brath, A. 2007 Comparing the performance of a 2-D finite element and a 2-D finite volume model of floodplain inundation using airborne SAR imagery. *Hydrol. Processes* **21**, 2745–2759.

Iervolino, P., Guida, R., Iodice, A. & Riccio, D. 2015 Flooding water depth estimation with high-resolution SAR. *IEEE Trans. Geosci. Remote Sens.* **53**, 2295–2307.

Kasischke, E. S. & Bourgeau-Chavez, L. L. 1997 Monitoring South Florida wetlands using ERS-1 SAR imagery. *Photogramm. Eng. Remote Sens.* **63**, 281–291.

Kittler, J. & Illingworth, J. 1986 Minimum error thresholding. *Pattern Recognition* **19** (1), 41–47. https://doi.org/10.1016/0031-3203(86)90030-0.

H2Open Journal Vol 3 No 1
doi: 10.2166/h2oj.2020.117

Kuenzer, C., Guo, H., Huth, J., Leinenkugel, P., Li, X. & Dech, S. 2013 Flood mapping and flood dynamics of the Mekong Delta: ENVISAT-ASAR-WSM based time series analyses. *Remote Sens.* **5**, 687–715.

Liu, Z., Merwade, V. & Jafarzadegan, K. 2018 Investigating the role of model structure and surface roughness in generating flood inundation extents using 1D and 2D hydraulic models. *J. Flood Risk Manage.* e12347. 10.1111/jfr3.12347.

Lu, J., Giustarini, L., Xiong, B., Zhao, L., Jiang, Y. & Kuang, G. 2014 Automated flood detection with improved robustness and efficiency using multi-temporal SAR data. *Remote Sens. Lett.* **5**, 240–248.

Martinis, S. & Rieke, C. 2015 Backscatter analysis using multi-temporal and multi-frequency SAR data in the context of flood mapping at River Saale, Germany. *Remote Sens.* **7**, 7732–7752.

Martinis, S., Twele, A. & Voigt, S. 2009 Towards operational near-real time flood detection using a split-based automatic thresholding procedure on high resolution TerraSAR-X data. *Nat. Hazards Earth Syst. Sci.* **9**, 303–314. https://doi.org/10.5194/nhess-9-303-2009.

Martinis, S., Kersten, J. & Twele, A. 2015 A fully automated TerraSAR-X based flood service. *ISPRS J. Photogramm. Remote Sens.* **4**, 203–212. https://doi.org/10.1016/j.isprsjprs.2014.07.014.

Matgen, P., Schumann, G., Henry, J. B., Hoffmann, L. & Pfister, L. 2007 Integration of SAR-derived river inundation areas, high-precision topographic data and a river flow model toward near real-time flood management. *Int. J. Appl. Earth Obs. Geoinf.* **9**, 247–263.

Matgen, P., Hostache, R., Schumann, G., Pfister, L., Hoffmann, L. & Savenije, H. 2011 Towards an automated SAR-based flood monitoring system: lessons learned from two case studies. *Phys. Chem. Earth Parts A/B/C* **36**, 241–252.

Moya Quiroga, V., Kure, S., Udo, K. & Mano, A. 2016 Application of 2D numerical simulation for the analysis of the February 2014 Bolivian Amazonia flood: application of the new HEC-RAS version 5. *Ribagua* **3** (1), 25–33. doi:10.1016/j.riba.2015.12.001.

Oberstadler, R., Hönsch, H. & Huth, D. 1997 Assessment of the mapping capabilities of ERS-1 SAR data for flood mapping: a case study in Germany. *Hydrol. Processes* **11**, 1415–1425.

Otsu, N. 1979 A threshold selection method from gray-level histograms. *IEEE Transactions on Systems, Man and Cybernetics* **9** (1), 62–66. doi:10.1109/TSMC.1979.4310076.

Parhi, P. K., Sankhua, R. N. & Roy, G. P. 2012 Calibration of channel roughness for Mahanadi River, (India) using HEC-RAS model. *J. Water Resour. Prot.* **4**, 847–850.

Pulvirenti, L., Pierdicca, N. & Chini, M. 2010 Analysis of COSMO-SkyMed observations of the 2008 flood in Myanmar. *Ital. J. Remote Sens.* **42**, 79–90.

Pulvirenti, L., Chini, M., Pierdicca, N., Guerriero, L. & Ferrazzoli, P. 2011 Flood monitoring using multi-temporal COSMO-SkyMed data: image segmentation and signature interpretation. *Remote Sens. Environ.* **115**, 990–1002. doi:10.1016/j.rse.2010.12.002.

Richards, J. A., Woodgate, P. W. & Skidmore, A. K. 1987 An explanation of enhanced radar backscattering from flooded forests. *Int. J. Remote Sens.* **8**, 1093–1100.

Schumann, G., Henry, J., Hoffmann, L., Pfister, L., Pappenberger, F. & Matgen, P. 2005 Demonstrating the high potential of remote sensing in hydraulic modelling and flood risk management. In: *Proceedings of the Annual Conference of the Remote Sensing and Photogrammetry Society with the NERC Earth Observation Conference*, 6–9 September 2005, Portsmouth, UK.

Schumann, G., Baldassarre, G. D., Alsdorf, D. & Bates, P. D. 2010 Near real-time flood wave approximation on large rivers from space: application to the River Po, Italy. *Water Resour. Res.* **46**, 1–8.

SENAGUA (SecretaríaNacionaldel Agua) 2014 *Vulnerability Assessment to Flood Events of the Santa Bárbara River*. Vol. 2. *Hydraulic Study*, ENAGUA, Quito, p. 108. (in Spanish).

Sezgin, M. & Sankur, B. 2004 Survey over image thresholding techniques and quantitative performance evaluation. *J. Electron. Imaging* **13**, 146–168. doi:10.1117/1.1631315.

Shastry, A. & Durand, M. 2019 Utilizing flood inundation observations to obtain floodplain topography in data-scarce regions. *Front. Earth Sci.* **6**, 243. doi:10.3389/feart.2018.00243.

Shen, X., Wang, D., Mao, K., Anagnostou, E. & Hong, Y. 2019 Inundation extent mapping by synthetic aperture radar: a review. *Remote Sens.* **11**, 879.

Surwase, T., SrinivasaRao, G., Manjusree, P., Begum, A., Nagamani, P. V. & JaiSankar, G. 2019 Flood inundation simulation of Mahanadi River, Odisha during September 2008 by using HEC-RAS 2D model. In: *Proceedings of International Conference on Remote Sensing for Disaster Management. Springer Series in Geomechanics and Geoengineering* (Rao, P., Rao, K. & Kubo, S., eds). Springer, Cham, Switzerland.

Tan, Q., Bi, S., Hu, J. & Liu, Z. 2004 Measuring lake water level using multi-source remote sensing images combined with hydrological statistical data. In: *Proceedings of the IGARSS'04, 2004 IEEE International Conference on Geoscience and Remote Sensing Symposium*, 20–24 September 2004, Anchorage, AK, USA, pp. 4885–4888.

Teng, J., Jakeman, A. J., Vaze, J., Croke, B., Dutta, D. & Kim, S. 2017 Flood inundation modelling: a review of methods, recent advances and uncertainty analysis. *Environ. Modell. Software* **90**, 201–216. doi:10.1016/j.envsoft.2017.01.006.

Tholey, N., Clandillon, S. & De Fraipont, P. 2015 The contribution of spaceborne SAR and optical data in monitoring flood events: examples in northern and southern France. *Hydrol. Processes* **11**, 1409–1413.

Townsend, P. 2002a Relationships between forest structure and the detection of flood inundation in forested wetlands using C-band SAR. *Int. J. Remote Sens.* **23**, 443–460.

Townsend, P. A. 2002b Estimating forest structure in wetlands using multitemporal SAR. *Remote Sens. Environ.* **79**, 288–304.

H_2Open Journal Vol 3 No 1
doi: 10.2166/h2oj.2020.117

Twele, A., Cao, W., Plank, S. & Martinis, S. 2016 Sentinel-1-based flood mapping: a fully automated processing chain. *Int. J. Remote Sens.* **37** (13), 2990–3004. https://doi.org/10.1080/01431161.2016.1192304.

Vala, H. J. & Baxi, A. 2013 A review on Otsu image segmentation algorithm. *Int. J. Advanc. Res. Comput. Eng. Technol.* **2** (2), 387–389.

Yamada, Y. 2001 Detection of flood-inundated area and relation between the area and micro-geomorphology using SAR and GIS. In: *Proceedings of the IGARSS'01, IEEE 2001 International Conference on Geoscience and Remote Sensing Symposium*, 9–13 July 2001, Sydney, NSW, Australia, pp. 3282–3284.

First received 21 February 2020; accepted in revised form 3 June 2020. Available online 22 July 2020